ORIGINAL ARTICLE

JBMR®

How Tough Is Brittle Bone? Investigating Osteogenesis Imperfecta in Mouse Bone

Alessandra Carriero,[1,2,3] Elizabeth A Zimmermann,[2,3] Adriana Paluszny,[4] Simon Y Tang,[5] Hrishikesh Bale,[2,3] Bjorn Busse,[2,3] Tamara Alliston,[5] Galateia Kazakia,[6] Robert O Ritchie,[2,3] and Sandra J Shefelbine[1]

[1]Department of Bioengineering, Imperial College, London, United Kingdom
[2]Materials Sciences Division, Lawrence Berkeley National Laboratory, Berkeley, CA, USA
[3]Department of Materials Science and Engineering, University of California Berkeley, Berkeley, CA, USA
[4]Department of Earth Science and Engineering, Imperial College, London, United Kingdom
[5]Department of Orthopaedic Surgery, University of California San Francisco, San Francisco, CA, USA
[6]Department of Radiology and Biomedical Imaging, University of California San Francisco, San Francisco, CA, USA

ABSTRACT

The multiscale hierarchical structure of bone is naturally optimized to resist fractures. In osteogenesis imperfecta, or brittle bone disease, genetic mutations affect the quality and/or quantity of collagen, dramatically increasing bone fracture risk. Here we reveal how the collagen defect results in bone fragility in a mouse model of osteogenesis imperfecta (*oim*), which has homotrimeric α1(I) collagen. At the molecular level, we attribute the loss in toughness to a decrease in the stabilizing enzymatic cross-links and an increase in nonenzymatic cross-links, which may break prematurely, inhibiting plasticity. At the tissue level, high vascular canal density reduces the stable crack growth, and extensive woven bone limits the crack-deflection toughening during crack growth. This demonstrates how modifications at the bone molecular level have ramifications at larger length scales affecting the overall mechanical integrity of the bone; thus, treatment strategies have to address multiscale properties in order to regain bone toughness. In this regard, findings from the heterozygous *oim* bone, where defective as well as normal collagen are present, suggest that increasing the quantity of healthy collagen in these bones helps to recover toughness at the multiple length scales. © 2014 American Society for Bone and Mineral Research.

KEY WORDS: BRITTLE BONE; BONE FRACTURE; FRACTURE MECHANICS; MOUSE BONE; CRACK INITIATION; CRACK GROWTH

Introduction

Bone is strong and tough because of its complex hierarchical composite structure with primarily collagen and hydroxyapatite (HA) as its constituents. The integrity of the bone at all levels of its hierarchical structure is of clinical importance for preserving bone function. In osteogenesis imperfecta (OI), or brittle bone disease, mutations at the molecular level result in bone fragility and spontaneous fracture at the whole bone level.

OI affects 1 in 15,000 births and currently has no cure.[1] Clinically, low bone mass and strength, extreme bone fragility, and skeletal deformities are characteristics of OI, resulting from a variety of mutations of type I collagen structure and quantity.[2–6] Histomorphometric analysis of the iliac crests from OI patients revealed reduced cortical and trabecular bone volume and increased osteoblast and osteoclast presence with increased bone turnover but reduced mineral apposition rate, which is not compensated by the increased cell number.[5,6] Fourier transform infrared spectroscopy (FTIR) and quantitative backscattered electron imaging of bones from OI patients show high mineral content and loss of mineralization heterogeneity.[6] All of these features, together with the poor collagen organization[7] and the high vascular canal density and connectivity,[8] contribute to the bone fragility in patients with OI.[1] An understanding of why the collagen molecular defect results in bone tissue fragility in OI is critical for developing therapies that can repair bone's mechanical integrity.

The OI murine (*oim)* model has been widely used to examine bone properties[9–17] and develop treatments.[18–22] *Oim* mice naturally produce α1(I) collagen homotrimers instead of normal heterotrimer α1(I)2α1(I) collagen, a similar collagen mutation seen in human OI,[23] and exhibit phenotypic and biochemical features typical of the disease.[10,16] Homozygous *oim* mice (*oim/oim*) have spontaneous skeletal fractures, acute osteopenia, bone deformities, and decreased body size.[10] *Oim/oim* cortical bone has increased mineralization with decreased

Received in original form October 11, 2013; revised form December 18, 2013; accepted January 9, 2014. Accepted manuscript online January 13, 2014.
Address correspondence to: Alessandra Carriero, PhD, Department of Bioengineering, Royal School of Mines, Imperial College, South Kensington Campus, SW7 2AZ, London, UK. E-mail: a.carriero@imperial.ac.uk
Additional Supporting Information may be found in the online version of this article.
ROR and SJS contributed equally to this work.
Journal of Bone and Mineral Research, Vol. 29, No. 6, June 2014, pp 1392–1401
DOI: 10.1002/jbmr.2172

heterogeneity,[9] increased woven bone,[10] and increased vascular and osteocyte lacunae density.[24] Long bones and vertebrae of *oim/oim* mice have inferior mechanical properties compared with healthy counterparts, including very little plastic deformation and reduced stiffness.[13,25,26] The heterozygous *oim* mice (*oim*/+) have the same collagen mutation but also have normal collagen.[16] As a result, bones from *oim*/+ mimic mild human OI with less severe osteopenia, no spontaneous fractures, and intermediate mechanical and morphological features between brittle *oim/oim* and healthy bone.[16]

Despite the body of research conducted on OI and *oim* bone, it is still unclear how structural and compositional changes through the hierarchy result in brittle bone. Here we investigate the mechanisms responsible for aberrant fracture resistance in *oim* bones. Specifically, we first measure bone toughness of *oim* homozygous, heterozygous, and healthy wild-type (WT) bones at the whole bone level. To explain differences in their crack-resistance behavior, we characterize crack propagation at the microscale within an environment scanning electron microscope (ESEM) and determine changes in bone in relation to the crack extension (crack-resistance curve or R-curve). To relate the crack path to the 3D intracortical architecture, we compare the nano-CT of *oim*/*oim*, *oim*/+, and WT of cracked bones and define the influence of vascular canal structure on crack extension and deviation by using finite element analysis. Then we determine the contribution of the bone constituents at the nanoscale to its fracture resistance by assessing the mechanical behavior of collagen fibrils and HA crystals using X-ray scattering and diffraction (SAXS/WAXD) patterns with the bone under tension. Finally, we associate mechanical changes with compositional changes at the bone tissue level and to cross-linking structural changes in the collagen. Through such a multiscale study, we are able to detect the salient damage modes and corresponding degradation in specific toughening mechanisms in *oim* bone that leads to its brittleness.

Materials and Methods

Bone test samples were taken from 10 homozygous mice B6C3Fe-a/aCol1a2$^{oim/oim}$ (*oim/oim*) model of severe OI, 10 heterozygous B6C3Fe-a/aCol1a2$^{oim/+}$ (*oim/+*) mice model of mild OI, and 10 wild-type B6C3Fe-a/a +/+ (WT or +/+) mice model of healthy bone from a maintained local colony. All mice were male and euthanized at 8 weeks old. The mice were fresh frozen after culling, and bones were dissected at the time of testing.

Fracture toughness

For toughness testing, right femora of the mice were dissected and machine micro-notched on the posterior surface of the mid-diaphysis with a razor blade irrigated with 0.05 μm diamond suspension; notch root radii with this technique consistently were less than 5 μm. Tests were performed in general accordance with American Society for Testing and Materials (ASTM) standards.[27] All samples were stored in Hank's balanced salt solution (HBSS)-soaked gauze at 25°C until testing (less than 12 hours). Consistent with ASTM standards,[27,28] a three-point bending configuration was used for the toughness tests with a displacement rate of 1 μm/s in 37°C HBSS bath. The toughness was calculated with the instability method, which accounts for the contributions to the toughness from the extension as well as the initiation of cracking.[29]

In situ fracture tests in an environmental scanning electron microscope (ESEM)

To identify the dominant sources of toughness in mouse bone and their contributions to the bone's resistance to the growth of cracks, we also performed fracture mechanics testing of healthy WT (+/+), *oim/oim*, and *oim/+* bones in situ in an ESEM. Left femora of five *oim/oim*, five *oim/+*, and five +/+ mice were dissected for testing. The periosteal surface of the femora was polished with 400-grit silicon carbide paper and then with increasingly higher finish until a final polish with 0.05 μm diamond suspension to make the osteocyte lacunae and the vascular canals visible within the ESEM (Hitachi S-4300SE/N ESEM, Hitachi America, Pleasanton, CA, USA). The samples were then machine micro-notched, as described above, and immersed in ambient HBSS for at least 12 hours before testing.

Crack propagation was observed on the bone surface in the ESEM while bones were tested moist in three-point bending at a rate of 1.6 μm/s at 25°C on the in situ loading stage (Gatan, Abington, UK). Images of the crack path were obtained simultaneously in back-scattered mode at 25 kV with a pressure of 35 Pa.

Fracture toughness values were calculated at each increment of stable crack extension so that crack-resistance curves (R-curves) for stable crack propagation in the mouse bone could be determined in terms of the stress-intensity factor, K,[29] and work of fracture, W_f, as a function of the crack extension, Δa. The work of fracture was defined as the work per unit area of fracture; it was determined from the area under the load-displacement curve divided by twice the area of the fracture surface at the point of measurement.

Synchrotron X-ray computed tomography

Synchrotron X-ray computed tomography (CT) was performed at the hard X-ray tomography beamline 8.3.2 of the Advanced Light Source (ALS, Lawrence Berkeley National Laboratory) to visualize the interaction in 3D between the vascular canal network of the bones and the crack path after R-curve testing. Bones were oriented with their longitudinal axis parallel to the stage rotation axis during scanning, and high-resolution 3D representations of the femoral mid-diaphysis of the bones and crack path were acquired for *oim/oim*, *oim/+*, and WT (+/+) bone using a nominal resolution of 0.9 μm at a photon energy of 18.25 keV. The data were reconstructed using filtered back-projection (Octopus software), and 3D morphology of the bone was binarized in ImageJ[30] through grayscale thresholding followed by binary operations of pixel dilation and erosion to eliminate artefacts from thresholding. The vascular canal network and crack were spatially decomposed into separate domains for 3D volumetric visualization (Avizo, Burlington, MA, USA).

In silico 3D fracture propagation modeling

We assessed the influence of vascular canal size and density on crack propagation in bone in silico using a 3D finite element model that explicitly models vascular canals, crack angle, and crack extension. A notched femoral shaft (approximated as a homogeneous, isotropic, linear elastic hollow cylinder, with elastic modulus $E = 20$ GPa and Poisson's ratio $\nu = 0.3$) was subjected to three-point bending displacement boundary conditions equivalent to applying a load of 2.1 N in the transverse direction at the bone mid-diaphysis (location of the notch). Three-dimensional fracture propagation was simulated

using an in-house linear elastic mesh-independent finite element model (C++ 3D Fracture propagation code based on the CSMP++ Mechanics library developed at Imperial College).[31]

Fracture behavior through the bone was modeled in presence of a single large vascular canal (diameter equal to a quarter of the cortical thickness) and in presence of eight smaller vascular canals (diameter equal to 1/16 of the cortical thickness) modeled as voids within the bone structure. Canals were defined using smooth parametric surfaces as part of the bone geometric model. Canals were modeled explicitly by the mesh and their interior is not meshed.

Fracture geometries were represented explicitly, and their growth was based on the step-by-step deformation of the bone matrix. At each growth step, the *J*-integral was applied to compute modal (tension – opening and shear) stress intensity factors at each element.[31] Energy-based growth, propagation, and angle criteria were used to predict growth extent and direction. An Irwin type law was used to evaluate failure in an iterative manner. At each iteration, relative growth increments along the tip were computed as a function of local stress-intensity factors.[32–35] At each step, the length advance at a given fracture tip location was defined as the maximum crack advance by a power of the ratio between the local strain energy release ratio and the maximum strain energy release. Maximum crack advance at each step was set to 1.3×10^{-5} mm and the exponent was equal to 4.5.[35] A maximum circumferential stress angle criterion determined the crack angle.[31]

The simulations were interaction-free with a crack surface geometric modification based on localized stress intensity factor and angle computations, and an automatic resolution adjustment of arbitrary tetrahedral mesh at each growth step.

In situ tensile testing with small-/wide-angle X-ray scattering/diffraction (SAXS/WAXD)

To examine the toughening behavior of *oim* bones at submicron length scales, we performed in situ high-flux synchrotron X-ray scattering experiments on *oim/oim*, *oim/+* and WT bone (ulna) while loaded uniaxially in tension. Ulnas of the same mice were dissected and wrapped in HBSS-soaked gauze for at least 12 hours before testing. The samples were mounted in a load frame positioned in beamline 7.3.3 at the ALS synchrotron radiation facility so that they were loaded in tension at a displacement rate of 1 μm/s in a custom-made rig with a 5-kg load cell (LC703-10, Omega Engineering, Stamford, CT, USA) while in situ SAXS/WAXD data were collected simultaneously with mechanical loading. Nanoscale fibril strain and mineral strain within the bone was determined at each level of externally applied load from shifts in the Bragg peak positions arising from the meridional axis of the collage fibril stagger and c-axis (002) of the HA mineral, taken at the small and wide scattering angle, respectively. The influence of radiation on mechanical testing was minimized by limiting the total X-ray exposure to 30 kGy.[36] Ulnas were exposed to X-rays for 0.5 seconds every 15 seconds during mechanical testing. Tests were conducted at 25°C on continuously hydrated samples. SAXS and WAXD data were collected simultaneously by a high-speed Pilatus detector and a Quantum CCD X-ray detector (Area Detector Systems Corporation, Poway, CA, USA), respectively, positioned at approximately 4100 and 250 mm from the bone. ESEM images of the bone cross-section permitted the measurement of the tissue stress. The applied load was normalized by the cross-sectional surface of the bone to calculate the tissue stress, whereas the tissue strain was determined by imaging the change in spacing of horizontal lines marked on the sample's surface; the displacement of these lines was then divided by the separation at zero loading to determine the bulk tissue strain. The images were analyzed with image analysis software (Vision Assistant 8.5, National Instruments, Austin, TX, USA). The software IGOR Pro (WaveMetrics, Tigard, OR, USA), used simultaneously with the custom macro NIKA (Jan Ilavsky, Argonne National Laboratory, Argonne, IL, USA), permitted the conversion of the scattering data from 2D to 1D. The sample-to-detector distance and beam center were calibrated with a silver behenate standard. The 2D SAXS and WAXD data were converted to 1D by radially integrating over a sector of 10° and a sector 20 pixels wide, respectively oriented parallel and perpendicular to the direction of loading.[37] The peaks of the first-order collagen fibril and the (0002) HA were found by fitting the 1D data sets with a Gaussian and a linear function.[37] Collagen fibrils strain and mineral strain were determined as the change in position of the corresponding peak's centre normalized by its location at zero loading (unstressed state sample).

Fourier transform infrared (FTIR) spectroscopy

The analysis of the FTIR absorbance band areas of the bone was conducted to reveal the difference in composition of the *oim* bones. Mid-diaphysis of right femora from fracture toughness tests were analyzed by FTIR spectroscopy. After testing, the bones were fixed in 70% ethanol. From each specimen, 2-mg (~2 mm long segment) of bone from the desired region was isolated, desiccated through a series of washes with increasing concentration of ethanol, and finally exposed in a desiccant chamber. A homogenized powder mixture was created of 1% bone by weight in potassium bromide (KBr; Thermo Electron, Waltham, MA, USA). A pellet for FTIR spectroscopy was created by compressing the powder mixture using a manual die. A benchtop interferometer system (Nexus 870, Thermo Electron) was used for performing spectroscopy, and 32 spectra scans at a spectral resolution of 4 cm^{-1} were acquired for each specimen. A background scan, recorded immediately after each sample scan, was subtracted for correction. The spectra were then analyzed with a custom-made code (Matlab, Mathworks, Natic, MA, USA) and double-checked with a chemical imaging software (Isys, Spectral Dimensions, Olney, MD, USA). Spectra were baseline-adjusted and the areas of the amide I (1595 to 1720 cm^{-1}), $\nu_1\nu_3$ phosphate (PO_4^{3-}, 895 to 1215 cm^{-1}), and ν_2 carbonate (CO_3^{2-}, 840 to 890 cm^{-1}) bands were integrated so that mineral-to-matrix (PO_4^{3-}/amide I) and carbonate-to-phosphate (CO_3^{2-}/PO_4^{3-}) ratios were calculated.

Accumulation of AGEs

The extent of the nonenzymatic cross-links, or advanced glycation end products (AGEs), present in the left tibias of the same mice, were evaluated using molecular florescence. The tibias were demineralized using ethylenediaminetetraacetic (EDTA) acid and then hydrolyzed using 6 N HCl for 24 hours at 110°C. AGEs content was determined by reading the natural bone fluorescence at the excitation wavelength of 370 nm and emission wavelength of 440 nm[38] (SpectraMax M5, Molecular Devices, Sunnyvale, CA, USA). These readings were then standardized to a quinine-sulphate standard and normalized to the amount of collagen present in each bone sample. The amount of collagen present in each sample was considered to be the amount of hydroxyproline contained into the bone and

determined using a chloramine-T colorimetric assay that recorded the absorbance of the hydrolysates against a commercially available hydroxyproline standard at the wavelength of 585 nm.[39]

Statistical analysis

Variables' homogeneity of variance and their normal distribution were analyzed by the Levene's test and the Shapiro-Wilk test, respectively (SPSS, IBM, Somers, NY, USA). Toughness, FTIR, and AGEs measures in WT, *oim/+*, and *oim/oim* bone were compared using analysis of variance (one-way independent ANOVA) because all the variables had normal distributions (SPSS). Variables were tested with post hoc procedures for multiple comparisons. All tests were two-tailed and, throughout the study, p values < 0.05 were considered to be significant.

Results

Fracture toughness

The toughness of ex vivo femoral cortical bone of *oim/oim*, *oim/+*, and WT (+/+) mice ($n = 10$/group, 8 weeks old) at the whole bone (macroscale) level is reported in Fig. 1*A*. Severe osteogenesis imperfecta (*oim/oim*) bone shows a dramatic 70% decrease in toughness compared with the normal counterpart (WT), whereas mild osteogenesis imperfecta (*oim/+*) showed a 30% decrease in toughness compared with healthy values.

In situ fracture tests in an ESEM

Crack-resistance curves (R-curves) for the growing stable cracks in such bone are plotted in Fig. 1*B, C* and presented in terms of measurements of crack-driving force, ie, the stress-intensity factor K, and energy absorbed, ie, the work to fracture W_f, as a function of the stable crack extension Δa. Results for the mouse cortical bone reveal a progressive loss in (i) stable crack extension, (ii) crack-initiation toughness (where $\Delta a \rightarrow 0$), and (iii) crack-growth toughness (slope of the R-curve), with severity of osteogenesis imperfecta (Fig. 1*B, C*). (We have used a constant displacement rate in this work to determine the R-curve toughness behavior; however, it should be noted that the magnitude of the toughness will likely diminish somewhat at higher displacement rates. This was not evaluated in this study. Toughness values were, however, insensitive to any small difference in hydration of the bones caused by testing HBSS-saturated femora in situ within the ESEM compared with the ex situ loading in HBSS.)

The extent of stable cracking is reduced by a factor of 2 in *oim/+* bone and by a factor of 4 in *oim/oim* bone compared with healthy WT bone, whereas crack-initiation toughness in *oim/+* and *oim/oim* is only, respectively, 30% and 65% of the value for healthy WT bone. The crack-growth toughness is large in WT bone as the toughness almost doubles its initial value at the end of the stable crack growth (~400 μm), whereas it is almost null (flat R-curve) in *oim* bones.

Real-time images of the crack profile for the three types of bone illustrated in Fig. 2*A* (details in Supplemental Fig. S1 and Supplemental Table S1) indicate that for WT bone, deflections in the crack path of ~60 to 90° run for hundreds of micrometers along the longitudinal direction of the bone, then restart their path in the transverse direction of the bone with an increased applied load or absorbed energy. These mechanisms result in extremely rough fracture surfaces (Fig. 2*B*) and high crack-growth toughness (high slope of R-curve) (Fig. 1*B, C*). In contrast, fractures in *oim/+* and *oim/oim* bone requires far lower driving force or energy to propagate (ie, a low slope of the R-curve) (Fig. 1*B, C*), consistent with the relative smooth fracture surfaces with little crack deflection (Fig. 2*B* and Supplemental Table S1).

Synchrotron X-ray computed tomography

Results presented in Fig. 3*A* show an increase in vascular canals within cortical *oim* bones with crack propagating transversally through vascular canals in both healthy and diseased murine bone. Three-dimensional crack paths are highly deflected in WT bone, whereas an almost flat and smooth crack is observed in *oim* bones.

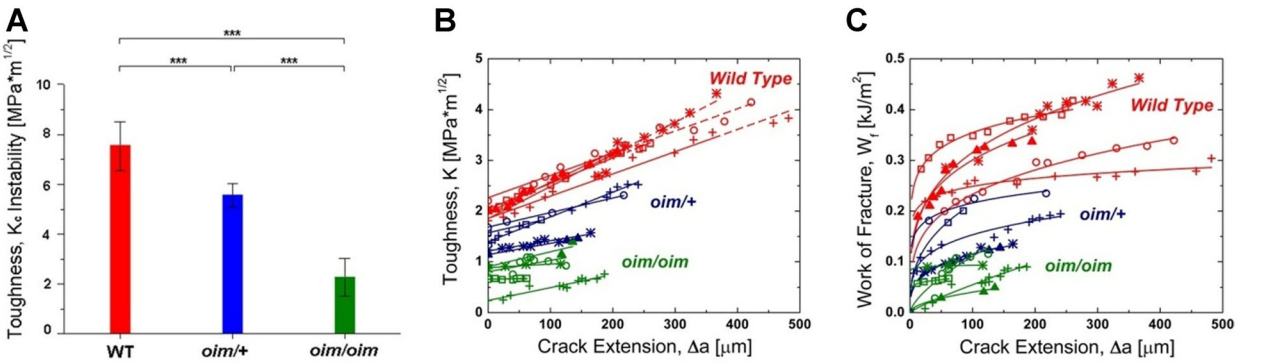

Fig. 1. Bone toughness and crack-resistance curves. (*A*) Critical values of in vitro instability fracture toughness properties of mouse cortical bone for healthy (red = WT) and mild (blue = *oim/+*) and severe osteogenesis imperfecta (green = *oim/oim*). Fracture toughness R-curve properties, in terms of (*B*) stress intensity K and (*C*) the work of fracture W_f, for WT, *oim/+*, and *oim/oim* bone show a reduced stable crack growth in *oim* bones. Crack-growth toughness (slope of R-curve) is high in WT and almost nonexistent in *oim* bones. Crack-initiation toughness (where $\Delta a \rightarrow 0$) in *oim/oim* and *oim/+* bone are, respectively, 30% and 60% of that of healthy bone ($^{***}p < 0.001$). In *B*, ASTM valid measurements are represented with a continuous line and ASTM invalid measurements with a dotted line.[27,28]

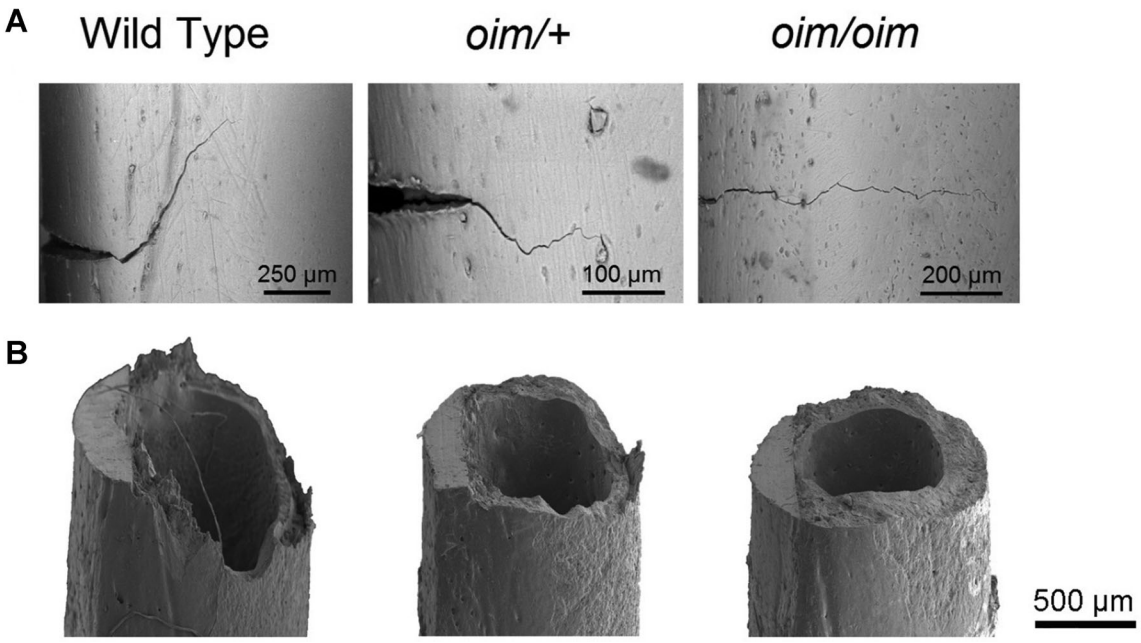

Fig. 2. Scanning electron micrographs of the crack path and fracture surface. (*A*) Crack paths in WT bone underwent multiple crack deflections, in conjunction with the through-thickness crack twists (*B*), resulting in a twofold increase in bone toughness with crack extension-rising R-curve behavior (Fig. 1*B, C*). Crack growth in *oim/+* and *oim/oim* bone displayed a much more linear crack path, contributing to ~25% of its toughness (Fig. 1*B, C*) and resulting in an almost flat fracture surface (*B*). (*B*) Rough deflected and twisted fracture surface in WT bone (in correspondence with its lamellar structure) contrasts the flat fracture surfaces in *oim* bones.

In silico 3D fracture propagation

Computational results showed that the crack propagates transversally through the vascular canals with little or no deflection in all scenarios (Supplemental Fig. S2). However, the crack propagates faster in the presence of smaller and more numerous vascular canals than in presence of a single large vascular canal; specifically, crack extension is 1.4 times larger in the presence of multiple small vascular canals compared with one large vascular canal (Supplemental Table S2).

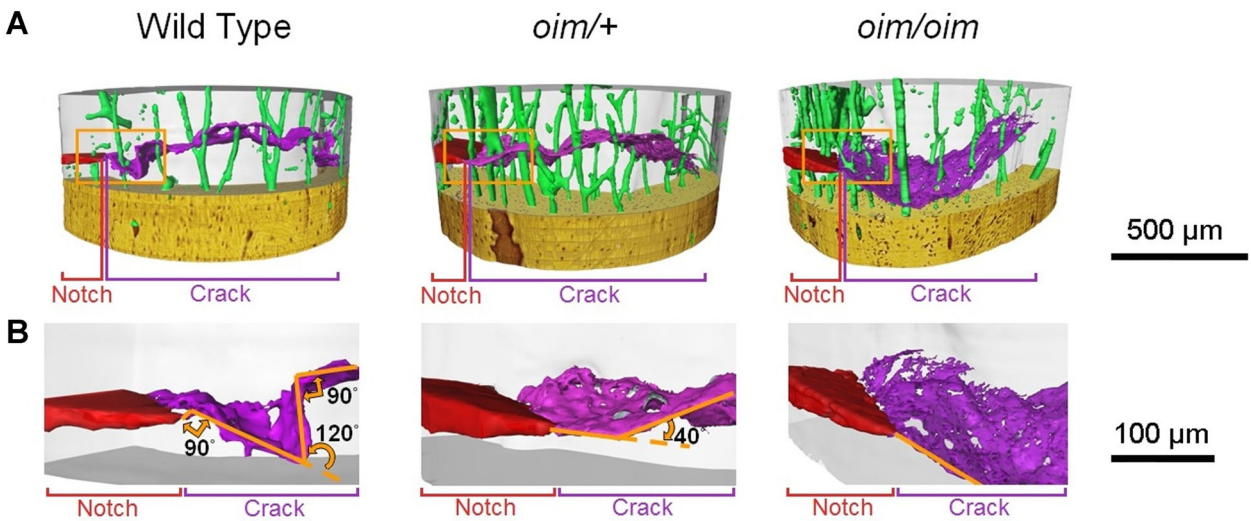

Fig. 3. Synchrotron X-ray reconstruction of 3D crack profile and vascular canal network. (*A*) Synchrotron X-ray computed tomography of WT, *oim/+*, and *oim/oim* bone shows 3D images of the crack profile (purple) during stable crack growth from a razor-sharpened micro-notch (red). Images show an increase in the vascular canals within cortical *oim* bones (green). In all cases, crack propagates transversally through the vascular canals. (*B*) Detail of the crack initiation in WT, *oim/+*, and *oim/oim* bone showing 90° to 120° deflections for WT bone and a smooth crack path in *oim* bones.

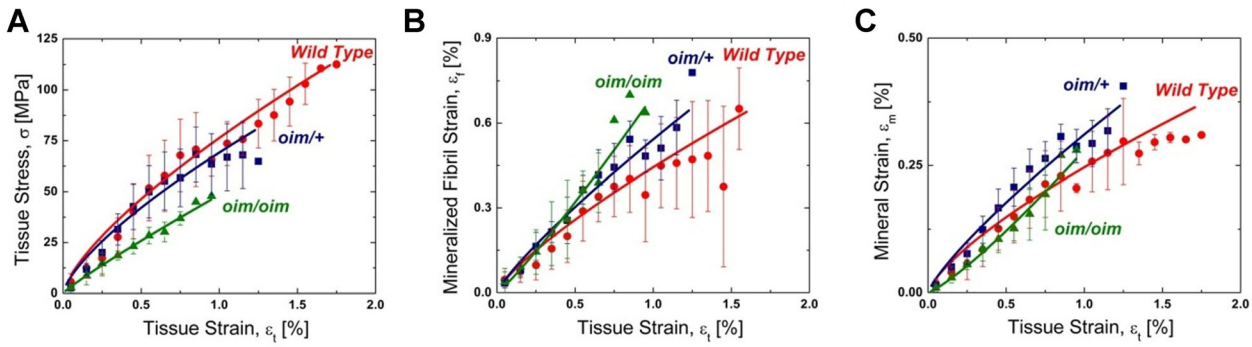

Fig. 4. Collagen fibril and mineral nanomechanics. (*A*) Tissue bone stress-strain curves for WT (red), *oim/+* (blue), and *oim/oim* (green) bone show reduced mechanical properties in *oim* bones. (*B, C*) Results for the SAXS and WAXD experiments during tensile tests show that at small tissue strain, the mineralized fibrils stretch more in the *oim* bones before break at only ~1% tissue strain compared with more than 1.5% tissue strains in healthy bone.

In situ SAXS/WAXD tensile tests

Figure 4*A* illustrates that *oim/oim* and *oim/+* bones are mechanically weaker than healthy bone, with a dramatic decrease in both ultimate tissue stress and strain. At small tissue strains, the curves are nearly identical for *oim/+* and healthy bone, but *oim/oim* bone is already significantly weaker. The ultimate (peak) stress is 40% and 67% of the normal healthy bone for the *oim/oim* and *oim/+* bone, respectively.

Figure 4*B, C* show the results from the simultaneous use of small-angle X-ray scattering (SAXS) and wide-angle X-ray diffraction (WAXD) techniques during in situ straining of the bone, which enables the partitioning of tissue strain between the mineralized collagen fibrils and the mineral crystals. At small tissue strains (<0.3%), the mineralized collagen fibril strain curves (Fig. 4*B*) are nearly identical for all bones. For tissue strains higher than 0.3%, the strain in the mineralized collagen fibrils is, respectively, 50% and 25% more in *oim/oim* and *oim/+* bone than in normal bone (Fig. 4*B*), implying that the fibrils are less stiff with disease severity. The corresponding strain carried by the mineral did not differ significantly with the state of disease (Fig. 4*C*).

FTIR spectroscopy

The analysis of the FTIR absorbance band showed that the *oim/oim* bone tissue has significantly higher mineral-to-matrix ratio with lower carbonate-to-phosphate ratio than the *oim/+* and healthy WT bone tissues (Fig. 5*A*, *B*). *Oim/+* bone has intermediate material composition and no significant differences in carbonate content compared with healthy bones (Fig. 6*A, B*).

Accumulation of AGEs

By using molecular fluorescence technique, we found a 30% increase of nonenzymatic cross-links, or AGEs,[40] in *oim/oim* bone compared with healthy bone (Fig. 6*C*). The AGEs content in the *oim* bones is underestimated in this study as the content of hydroxylisine is higher in homotrimer collagen than in the heterotrimer collagen;[41] therefore, there is actually less collagen than estimated in *oim* bones, suggesting a greater difference in AGEs content between *oim* and WT bone.

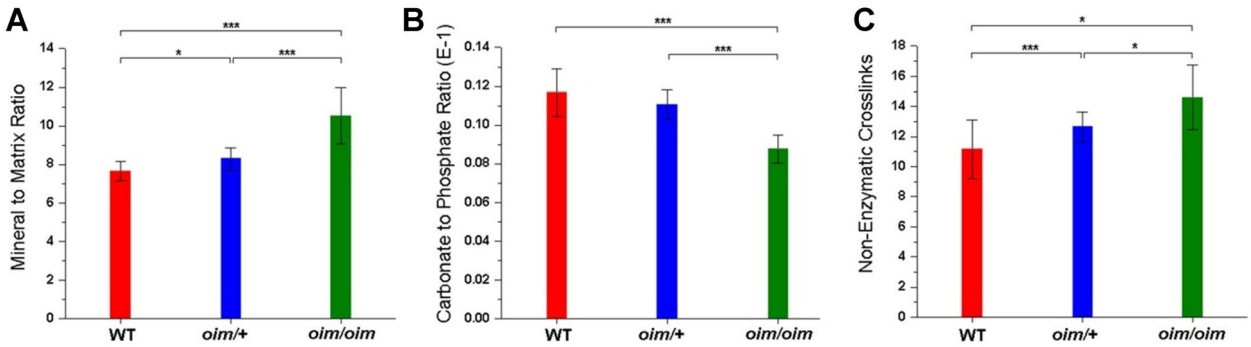

Fig. 5. Bone mineral composition and collagen nonenzymatic cross-links. (*A*) Mineral-to-matrix ratio and (*B*) carbonate-to-phosphate ratio obtained by scanning pellets of femoral mid-diaphysis bone for WT (red), *oim/+* (blue), and *oim/oim* (green) bone using FT infrared spectroscopy technique show a 40% increase in mineralization in *oim/oim* bone, with a 25% reduction in the carbonate content compared with WT bone. (*C*) AGEs accumulation fluorimetrically quantified in the tibias of WT (red), *oim/+* (blue), and *oim/oim* (green) mouse bone is 30% greater in *oim* bone ($^{***}p < 0.001$ and $^{*}p < 0.05$).

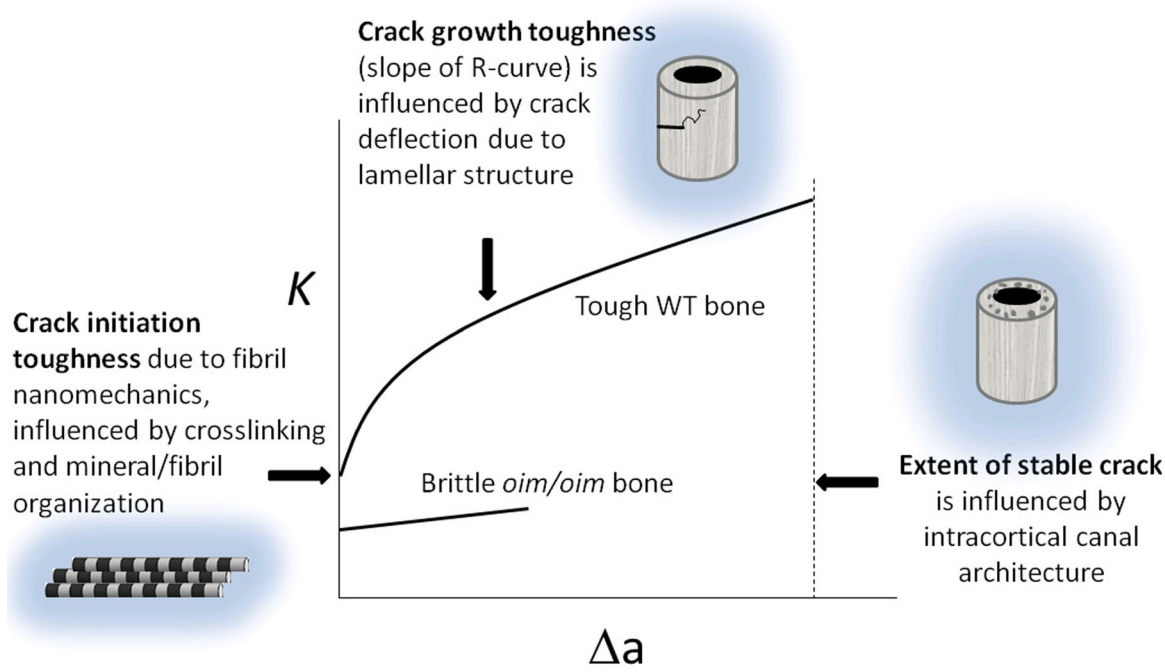

Fig. 6. Schematic of bone toughness (*K*) versus crack extension (Δ*a*). Schematic exemplifying the bone hierarchical structural feature contributing to its toughness in healthy and brittle mouse bone.

Discussion

Bone fragility in OI has been primarily attributed to osteopenia and low bone strength caused by the collagen mutations.[1] Here we reveal how collagen defects in OI deleteriously influence aspects of bone quality reducing the toughening mechanisms of bone at the multiple length-scales and hence increasing bone fragility at the organ level. Such information is important for the understanding of OI disease and for the development of novel treatment strategies to manage or cure patients with brittle bones.

Crack path and resistance to crack growth

Fracture toughness values from three-point bending tests of notched femurs showed reduced mechanical properties in *oim* bones, in agreement with findings in human OI biopsies.[7] By measuring the resistance-curve behavior for stable growing cracks in mouse bone, we were able to relate the resulting bone toughness to the nature of the crack trajectory during bending in WT and *oim* bones. First, from the R-curves, we can see that the crack extension is far less stable in *oim* bones than in healthy WT bone, indicating that a small crack in *oim* bones quickly progresses to unstable fracture and failure. One reason for this may be the bone porosity. Previous studies conducted on ex vivo human cortical bone have demonstrated that cortical porosity can be crucial for bone toughness, with the toughness negatively related to high intracortical porosity.[42,43] Our in situ ESEM images of crack propagation and ex situ 3D synchrotron X-ray tomographic reconstructions of crack propagation through the *oim* and WT bones indicate that cracks propagate transversally through vascular canals in both healthy and *oim* bone. Although *oim/oim* and WT bone have similar cortical porosity, the vascular canal density in *oim/oim* bone is 4.5 times higher with more small vascular canals that are highly branched.[24] A similar configuration has been found in human OI samples, where vascular canals had increased density and connectivity compared with healthy bones.[8] Our in silico 3D fracture propagation model of the bone with the vascular canals explicitly modeled indicates that in an isotropic medium, intracortical vascular canals have little influence on the deflection of the crack, but small vascular canals may reduce stable crack extension. Thus, when the crack is growing in *oim/oim* and OI bone, many small vascular canals can interrupt the continuity of the bone material and reduce its capacity to resist the crack propagation, decreasing the overall extension of the stable crack and facilitating its failure.

Coupled with the limited extent of stable crack extension, the slope of the R-curve is also low in *oim* bones. The degree of toughening of mouse bone is influenced by microscale toughening mechanisms, such as crack deflection. High-resolution ESEM images of the crack propagation and of the fracture surface together with synchrotron tomographic reconstructions show that crack trajectories are highly deflected out of and in the notch plane (crack twist) in healthy bone. Crack deflection and twisting are extrinsic toughening mechanisms,[44] which are a characteristic of healthy human bone, principally where propagating cracks interact with the cement lines of the osteons.[44–46] Mouse bones do not have osteons or Haversian canals; the highest level of organization of their bone is in concentric lamellae around their medullary cavity.[16] Studies conducted on human and other mammalian bones showed that the large number of interfaces between the lamellar structure of the bone can give rise to toughness mechanisms, such as crack deflection[47,48] and twisting.[45] Results from our study suggest

that the lamellae in healthy mouse bone act as delamination barriers, causing deflections and twist of the crack. In human bone, it is estimated that a single crack deflection of 90° can halve the stress intensity at the crack tip, thereby essentially doubling the fracture toughness.[45] Any combination of deflection with twisting of the crack can potentially further increase the toughness of bone.[45] These toughening mechanisms are consistent with the twofold increase in toughness during crack growth of the healthy WT bone found in this study, and their absence in *oim/oim* bone contributes to the reduced crack-growth toughness in brittle bone. Histological[10,16] and ultrasound critical-angle reflectometry[49] studies have revealed an increased woven bone content in *oim/oim* and *oim/+* bone. As previously postulated by Jepsen and colleagues[48,50] when analyzing fracture surface of Mov13 mouse bone (another model of mild OI), the reduced presence of lamellae in *oim* bones may explain the absence of crack deflections and twist in these bones. This, in turn, can explain their almost flat R-curves, which indicate an almost total lack of extrinsic toughening in *oim* bones. The significance of this is that once a crack nucleates in *oim* bones, with such minimal resistance to crack propagation, unstable cracking immediately ensues, leading to a complete fracture of the bone. We expect cracks to propagate smoothly without deflections in human OI bone because the weak interfaces between osteons can be comparable to the poorly organized collagen.[7]

Finally from the R-curves, it is noticeable that *oim* bones have markedly low crack-initiation toughness. Resistance to crack initiation is a function of intrinsic toughening, which is principally associated with plastic (or more correctly, inelastic) deformation, the origin of which in bone is primarily related to mechanisms of fibrillar sliding acting at submicron to nanoscale structural size scales,[44] as discussed below.

Collagen and mineral contribution to toughness

Our SAXS/WAXD results combined with tensile testing revealed that mineralized fibrils are less stiff with increasing severity of disease. For the stiffness of the mineralized fibrils to change within brittle *oim* bones, structural and compositional changes must occur in the collagen and mineral. Increased mineralization in the *oim/oim* compared with the *oim/+* and WT bones was revealed by our FTIR analysis, in agreement with previous studies.[20,51] The higher mineralization may promote the occurrence of microcracks,[52] which may explain (i) the elevated bone turnover of *oim* bones,[12,53] as the bone attempts to remove microcracks, and, consequently, (ii) the reduced carbonate content, as carbonate is typically incorporated as crystals mature.

The high mineralization and low ultimate strength observed in *oim/oim* bone may appear to be a contradiction. In normal bone, a well-established correlation exists between mineral content and strength[54] and stiffness,[55] which has been proposed to be caused by an end-to-end fusion of the apatite crystals.[55] However, because *oim/oim* bone has small and disorganized apatite crystals[25] with low crystallinity,[9] it is possible that the defective quality of mineral present in *oim/oim* bone prohibits normal fusion of crystals into a contiguous structure.[26]

The structural changes in the mineral result from the improper folding and kinks in the $\alpha(1)$ homotrimeric *oim* collagen molecule,[56] which cause a disruption of the fibril alignment and structure,[57,58] thereby providing an abnormal scaffold for mineral deposition. *Oim/oim* bone has 27% fewer stabilizing intermolecular enzymatic collagen cross-links (hydroxylysino-keto-norleucine or HLKNL);[17] a decrease in such enzymatic cross-links is known to decrease the mechanical strength of bone.[59] Using molecular fluorescence, we further reveal in this study an increase of nonenzymatic cross-links in *oim/oim* bone compared with healthy bone, probably as a consequence of the high oxidative stress induced by renal dysfunction in *oim* mice.[60] The accumulation of AGEs is known to deteriorate the mechanical properties of normal bone, increasing its stiffness and reducing its ductility.[40,61,62] In *oim* bone, aberrant cross-links may contribute to bone tissue fragility, already altered by abnormal enzymatic cross-linking.[63] However, mineralized fibril (shown here) and bone tissue[25] are less stiff in *oim* than in WT mice. Thus, it is possible that at low tissue strain, AGEs compensate for the reduction in stabilizing enzymatic cross-links, slightly increasing the stiffness and strength of the *oim* bone. In any case, both enzymatic and nonenzymatic cross-links are insufficient to maintain mechanical integrity and break prematurely without manifesting plasticity at the nanoscale dimension. Although further studies need to precisely elucidate the correlation between cross-linking and mechanical properties of murine bone, results from this study suggest that these cross-link modifications contribute to the increased fragility of the *oim* bone at the fibril and tissue level (Fig. 4*A, B*).

In healthy bone, the number and type of cross-links allow collagen fibrils to slide with respect to each other and/or stretch under mechanical forces.[37] In *oim/oim* bone with compromised collagen, its defective mineralized fibrils show large deformations at low tissue strains ($>0.3\%$) but with no further ability to extend at larger tissue strains. Specifically, the *oim/oim* fibrils fail at smaller ultimate tissue strains, resulting in a catastrophically brittle bone. When the same external forces are applied to healthy bone, the normal collagen fibrils are able to withstand these strains without failure; the resulting deformation then contributes markedly to the bone tissue toughness. These results show that fibril packing and intermolecular cross-linking are critical for maintaining mechanical strength and plasticity of the bone because initiation fracture toughness depends on the association between collagen fibrils and crystals.

Conclusions and clinical implications

This work provides an improved understanding of fracture in OI mouse bone and may offer insight for more effective treatment strategies for preventing bone fragility. The findings from this study indicate how collagen defects in *oim* alter bone structure and mechanical integrity. The hierarchical structure of healthy cortical bone, in mouse as well as in human bone, is naturally optimized to resist fracture. In this study, we show that in healthy mouse bone, three features of its hierarchical structure particularly influence its mechanical properties: (i) collagen fibrils with effective cross-links and organized mineralization at submicron level, which increases bone plasticity, (ii) vascular canal density, which influences crack propagation, and (iii) the lamellar structure of bone, which increases bone toughness by shielding the crack propagation with crack deflection and twisting (Fig. 6). The absence of the $\alpha 2$(I) chain of collagen in *oim/oim* bone results in altered fibril packing and intermolecular cross-linking: stabilizing enzymatic cross-links are missing while AGEs form. This generates an abnormal template for bone mineralization and affects the biomechanical quality of *oim/oim* bone tissue decreasing its plasticity. At microscopic length-scales, the high vascular canal density and the woven fibers of

oim bone provide little shielding to resist crack propagation. These findings provide guidance as to where therapeutic targets should be focused to increase toughness in bone.

Current treatments of the OI rely on bisphosphonate injection and exercise management. Both can increase the amount of bone but not its quality.[1] Findings from our *oim/+* group suggest that treatment strategies for OI should aim to increase the quantity of healthy collagen in these bones. In *oim/+* bone, the coexistence of normal and abnormal collagen packing also reduces bone plasticity and toughness but helps to avoid spontaneous fractures. In this sense, cellular therapy may offer a viable treatment to improve bone quality by delivering healthy cells to the affected bone, which produces healthy collagen that in turn restores lamellar structure. Further studies need to be conducted to introduce cellular approaches into clinical trials for OI patients in the future.

These findings have implications for many bone diseases, where treatments have largely focused on enhancing the mineral quantity and density of bone. However, in bones where quality is an issue, collagen plays an important role and treatments should aim to improve the collagen fibril packing, collagen fiber organization, and the interaction of collagen with the mineral. Therapies based on collagen chaperones and stem cells may represent the treatment for the future to improve collagen fibrillogenesis, regain organization at the fibril level, and create thick and strong fibers. Increasing the amount of good-quality collagen within these bones will serve to improve its bone tissue quality and reduce their fragility.

Disclosures

All authors state that they have no conflicts of interests.

Acknowledgments

The authors to thank Dr Joel Ager (LBNL) for his initial help with setting up the SAXS experiments, Drs Eric Schaible and Bernd Gludovatz (LBNL) for helping perform these experiments, and Mr Brian Panganiban (UC Berkeley) for his initial assistance with the mechanical testing. This work was largely performed at the LBNL, where it was supported by the Laboratory Directed Research and Development Program, funded by the US Department of Energy under contract no. DE-AC02-05CH11231. Funding for AC was provided by the Royal Academy of Engineering, UK; for SJS by the Elsie Widdowson Foundation, UK; and for GK by K01AR056734. We acknowledge the use of the two X-ray synchrotron beamlines 7.3.3 (SAXS/WAXD) and 8.3.2 (microtomography) at the ALS (LBNL), which are also supported by the Office of Science of the US Department of Energy under the same contract.

Authors' roles: AC jointly conceived the study with ROR and SJS. SJS provided the mice for the study. AC prepared the samples and performed and analyzed the data of the fracture toughness. AC and EAZ designed and performed the R-curve measurements and SAXS-WAXS experiments, and analyzed the data with the supervision of ROR. AP implemented the simulation models of bone fracture and analyzed them with AC. SYT and TA performed and analyzed the data about the AGE content in bone. HB performed the synchrotron X-ray tomography and analyzed the data with AC. AC, BB, and GK performed and analyzed the composition of bone. AC performed the statistical analysis. AC interpreted the data and wrote the manuscript with the supervision of ROR and SJS. EAZ, AP, SYT, HB, BB, TA, and GK revised the manuscript. All approved the final version of the manuscript.

References

1. Forlino A, Cabral WA, Barnes AM, Marini JC. New perspectives on osteogenesis imperfecta. Nat Rev Endocrinol. 2011;7:540–57.
2. Cole WG. The Nicholas Andry Award-1996. The molecular pathology of osteogenesis imperfecta. Clin Orthop Relat Res. 1997;343:235–48.
3. Cole WG. Advances in osteogenesis imperfecta. Clin Orthop Relat Res. 2002;401:6–16.
4. Rauch F, Glorieux FH. Osteogenesis imperfecta. Lancet. 2004;363 (9418):1377–85.
5. Rauch F, Travers R, Parfitt AM, Glorieux FH. Static and dynamic bone histomorphometry in children with osteogenesis imperfecta. Bone. 2000;26(6):581–9.
6. Traub W, Arad T, Vetter U, Weiner S. Ultrastructural studies of bones from patients with osteogenesis imperfecta. Matrix Biol. 1994;14: 337–45.
7. Alman B, Frasca P. Fracture failure mechanisms in patients with osteogenesis imperfecta. J Orthop Res. 1987;5(1):139–43.
8. Jameson J, Albert C, Busse B, Smith P, Harris G. 3D micron-scale imaging of the cortical bone canal network in human osteogenesis imperfecta (OI). Proc SPIE 8672, Medical Imaging 2013: Biomedical Applications in Molecular, Structural, and Functional Imaging. 2013 Mar 29.
9. Fratzl P, Paris O, Klaushofer K, Landis WJ. Bone mineralization in an osteogenesis imperfecta mouse model studied by small-angle x-ray scattering. J Clin Invest. 1996;97:396–402.
10. Chipman SD, Sweet HO, McBride DJ Jr, et al. Defective pro alpha 2(I) collagen synthesis in a recessive mutation in mice: a model of human osteogenesis imperfecta. Proc Natl Acad Sci USA. 1993;90(5):1701–5.
11. Grabner B, Landis WJ, Roschger P, et al. Age- and genotype-dependence of bone material properties in the osteogenesis imperfecta murine model (oim). Bone. 2001;29(5):453–7.
12. Kalajzic I, Terzic J, Rumboldt Z, et al. Osteoblastic response to the defective matrix in the osteogenesis imperfecta murine (oim) mouse. Endocrinology. 2002;143(5):1594–601.
13. McBride DJ Jr, Shapiro JR, Dunn MG. Bone geometry and strength measurements in aging mice with the oim mutation. Calcif Tissue Int. 1998;62(2):172–6.
14. Miller E, Delos D, Baldini T, Wright TM, Pleshko Camacho N. Abnormal mineral-matrix interactions are a significant contributor to fragility in oim/oim bone. Calcif Tissue Int. 2007;81:206–14.
15. Phillips CL, Bradley DA, Schlotzhauer CL, et al. Oim mice exhibit altered femur and incisor mineral composition and decreased bone mineral density. Bone. 2000;27(2):219–26.
16. Saban J, Zussman MA, Havey R, Patwardhan AG, Schneider GB, King D. Heterozygous oim mice exhibit a mild form of osteogenesis imperfecta. Bone. 1996;19(6):575–9.
17. Sims TJ, Miles CA, Bailey AJ, Camacho NP. Properties of collagen in OIM mouse tissues. Connect Tissue Res. 2003;44:202–5.
18. Vanleene M, Shefelbine SJ. Therapeutic impact of low amplitude high frequency whole body vibrations on the osteogenesis imperfecta mouse bone. Bone. 2013;53:507–14.
19. Guillot PV, Abass O, Bassett JH, et al. Intrauterine transplantation of human fetal mesenchymal stem cells from first-trimester blood repairs bone and reduces fractures in osteogenesis imperfecta mice. Blood. 2008;111:1717–25.
20. Vanleene M, Saldanha Z, Cloyd KL, et al. Transplantation of human fetal blood stem cells in the osteogenesis imperfecta mouse leads to improvement in multiscale tissue properties. Blood. 2011;117 (3):1053–60.
21. Rao SH, Evans KD, Oberbauer AM, Martin RB. Bisphosphonate treatment in the oim mouse model alters bone modeling during growth. J Biomech. 2008;41(16):3371–6.
22. Bargman R, Huang A, Boskey AL, Raggio C, Pleshko N. RANKL inhibition improves bone properties in a mouse model of osteogenesis imperfecta. Connect Tissue Res. 2010;51(2):123–31.

23. Nicholls AC, Osse G, Schloon HG, et al. The clinical features of homozygous alpha 2(I) collagen deficient osteogenesis imperfecta. J Med Genet. 1984;21(4):257–62.
24. Carriero A, Doube M, Levchuck A, Schneider P, Muller R, Shefelbine SJ. Cortical tissue porosity of brittle osteogenesis imperfecta bone. Presented at: 57th Annual Meeting of the Orthopaedic Research Society; January 13–16, 2011; Long Beach, CA.
25. Vanleene M, Porter A, Guillot PV, Boyde A, Oyen M, Shefelbine S. Ultra-structural defects cause low bone matrix stiffness despite high mineralization in osteogenesis imperfecta mice. Bone. 2012;50:1317–23.
26. Camacho NP, Hou L, Toledano TR, et al. The material basis for reduced mechanical properties in oim mice bones. J Bone Miner Res. 1999;14:264–72.
27. ASTM_E1820-09. Standard test method for measurement of fracture toughness. Annual book of Americal Society for Testing and Material Standards. West Conshohocken, PA: ASTM International; 2006.
28. ASTM_D790-10. Standard test method for flexural properties of reinforced plastics and electrical insulation materials. Annual book of Americal Society for Testing and Material Standards. West Conshohocken, PA: ASTM International; 2010.
29. Ritchie RO, Koester KJ, Ionova S, Yao W, Lane NE, Ager JW 3rd. Measurement of the toughness of bone: a tutorial with special reference to small animal studies. Bone. 2008;43:798–812.
30. Schneider CA, Rasband WS, Eliceiri KW. NIH Image to ImageJ: 25 years of image analysis. Nat Methods. 2012;9(7):671–5.
31. Paluszny A, Zimmerman RW. Numerical simulation of multiple 3D fracture propagation using arbitrary meshes. Comput Methods Appl Mech Eng. 2011;200:953–66.
32. Taylor D, Prendergast PJ. A model for fatigue crack propagation and remodelling in compact bone. Proc Inst Mech Eng H. 1997;211 (5):369–75.
33. Taylor D, Lee TC. Microdamage and mechanical behaviour: predicting failure and remodelling in compact bone. J Anat. 2003;203(2):203–11.
34. Taylor D, Tilmans A. Stress intensity variations in bone microcracks during the repair process. J Theor Biol. 2004;229:169–77.
35. Wright TM, Hayes WC. The fracture mechanics of fatigue crack propagation in compact bone. J Biomed Mater Res. 1976;10:637–48.
36. Barth HD, Launey ME, MacDowell AA, Ager JW, Ritchie RO. On the effect of X-ray irradiation on the deformation and fracture behavior of human cortical bone. Bone. 2010;46:1475–85.
37. Gupta HS, Seto J, Wagermaier W, Zaslansky P, Boesecke P, Fratzl P. Cooperative deformation of mineral and collagen in bone at the nanoscale. Proc Natl Acad Sci USA. 2006;103:17741–6.
38. Sell DR, Monnier VM. Isolation, purification and partial characterization of novel fluorophores from aging human insoluble collagen-rich tissue. Connect Tissue Res. 1989;19(1):77–92.
39. Woessner JF Jr. The determination of hydroxyproline in tissue and protein samples containing small proportions of this imino acid. Arch Biochem Biophys. 1961;93:440–7.
40. Saito M, Marumo K. Collagen cross-links as a determinant of bone quality: a possible explanation for bone fragility in aging, osteoporosis, and diabetes mellitus. Osteoporos Int. 2010;21:195–214.
41. Miles CA, Sims TJ, Camacho NP, Bailey AJ. The role of the alpha2 chain in the stabilization of the collagen type I heterotrimer: a study of the type I homotrimer in oim mouse tissues. J Mol Biol. 2002;321:797–805.
42. Bell KL, Loveridge N, Power J, Garrahan N, Meggitt BF, Reeve J. Regional differences in cortical porosity in the fractured femoral neck. Bone. 1999;24(1):57–64.
43. Yeni YN, Brown CU, Wang Z, Norman TL. The influence of bone morphology on fracture toughness of the human femur and tibia. Bone. 1997;21(5):453–9.
44. Launey ME, Buehler MJ, Ritchie RO. On the mechanistic origins of toughness in bone. Ann Rev Mater Res. 2010;40:25–53.
45. Koester KJ, Ager JW, Ritchie RO. The true toughness of human cortical bone measured with realistically short cracks. Nat Mater. 2008;7:672–7.
46. Zimmermann EA, Schaible E, Bale H, et al. Age-related changes in the plasticity and toughness of human cortical bone at multiple length scales. Proc Natl Acad Sci USA. 2011;108:14416–21.
47. Peterlik H, Roschger P, Klaushofer K, Fratzl P. From brittle to ductile fracture of bone. Nat Mater. 2006;5(1):52–5.
48. Jepsen KJ, Goldstein SA, Kuhn JL, Schaffler MB, Bonadio J. Type-I collagen mutation compromises the post-yield behavior of Mov13 long bone. J Orthop Res. 1996;14(3):493–9.
49. Mehta SS, Antich PP, Landis WJ. Bone material elasticity in a murine model of osteogenesis imperfecta. Connect Tissue Res. 1999;40 (3):189–98.
50. Jepsen KJ, Schaffler MB, Kuhn JL, Goulet RW, Bonadio J, Goldstein SA. Type I collagen mutation alters the strength and fatigue behavior of Mov13 cortical tissue. J Biomech. 1997;30(11–12):1141–7.
51. Camacho NP, Landis WJ, Boskey AL. Mineral changes in a mouse model of osteogenesis imperfecta detected by Fourier transform infrared microscopy. Connect Tissue Res. 1996;35(1–4):259–65.
52. Wasserman N, Yerramshetty J, Akkus O. Microcracks colocalize within highly mineralized regions of cortical bone tissue. Eur J Morphol. 2005;42:43–51.
53. Li H, Jiang X, Delaney J, et al. Immature osteoblast lineage cells increase osteoclastogenesis in osteogenesis imperfecta murine. Am J Pathol. 2010;176:2405–13.
54. Currey JD. The mechanical consequences of variation in the mineral content of bone. J Biomech. 1969;2(1):1–11.
55. Currey JD. The relationship between the stiffness and the mineral content of bone. J Biomech. 1969;2(4):477–80.
56. Chang SW, Shefelbine SJ, Buehler MJ. Structural and mechanical differences between collagen homo- and heterotrimers: relevance for the molecular origin of brittle bone disease. Biophys J. 2012;102:640–8.
57. Cole WG. The Nicholas Andry Award-1996. The molecular pathology of osteogenesis imperfecta. Clin Orthop Relat Res. 1997(343):235–48.
58. Cole WG. Advances in osteogenesis imperfecta. Clin Orthop Relat Res. 2002; (401):6–16.
59. Knott L, Whitehead CC, Fleming RH, Bailey AJ. Biochemical changes in the collagenous matrix of osteoporotic avian bone. Biochem J. 1995;310:1045–51.
60. Phillips CL, Pfeiffer BJ, Luger AM, Franklin CL. Novel collagen glomerulopathy in a homotrimeric type I collagen mouse (oim). Kidney Int. 2002;62:383–91.
61. Vashishth D. The role of the collagen matrix in skeletal fragility. Curr Osteoporos Rep. 2007;5(2):62–6.
62. Wang X, Shen X, Li X, Agrawal CM. Age-related changes in the collagen network and toughness of bone. Bone. 2002;31(1):1–7.
63. Coleman RM, Aguilera L, Quinones L, Lukashova L, Poirier C, Boskey A. Comparison of bone tissue properties in mouse models with collagenous and non-collagenous genetic mutations using FTIRI. Bone. 2012;51(5):920–8.